Characterization of thermal cross-talk in a MEMS-based thermopile detector array

2009 J. Micromech. Microeng. 19 074022

(http://iopscience.iop.org/0960-1317/19/7/074022)

J. Micromech. Microeng. **19** (2009) 074022 (7pp) doi:10.1088/0960-1317/19/7/074022

Characterization of thermal cross-talk in a MEMS-based thermopile detector array

H Wu, S Grabarnik, A Emadi, G de Graaf and R F Wolffenbuttel

Delft University of Technology, Faculty of EEMCS, Department of ME/EI, Mekelweg 4, 2828 CD Delft, The Netherlands

E-mail: H.W.Wu@tudelft.nl

Received 21 December 2008, in final form 4 March 2009
Published 30 June 2009
Online at stacks.iop.org/JMM/19/074022

Abstract

The spectral resolution of a MEMS-based IR microspectrometer critically depends on the thermal cross-talk between adjacent TE elements in the detector array. Thermal isolation between elements is realized by using bulk micromachining directly following CMOS processing. This paper reports on the characterization results of bridge-shaped TE detector elements that are cut out of a membrane. Elements with dimensions of 650 $\times$ 36 μm^2 are separated by 10 μm wide gaps in order to minimize the thermal cross-talk by heat conduction through the support structure. The static and dynamic aspects of thermal cross-talk have been evaluated with an emphasis on the effect of the thermal conductivity of air as a function of the package pressure.

(Some figures in this article are in colour only in the electronic version)

1. Introduction

Optical spectroscopy in the infrared (IR) spectral range has applications in agriculture, the food industry, soil biology, remote sensing and the chemical industry. Optical microspectrometers based on IC-compatible MEMS technologies offer significant benefits in these applications due to small sample volume, fast response, small dimensions and weight and integrated circuits for signal pre-processing [1]. The structure of the IR microspectrometer discussed in this paper comprises slit, planar imaging diffraction grating and thermo-electric (TE) detector array [2]. The dispersed IR spectrum is projected onto a one-dimensional detector array. The position of a spectral component within the IR spectrum is determined by the position of the element in the array. The response in terms of generated heat due to absorbed IR radiation at that particular element is a measure of the optical power within that part of the spectrum. The resulting localized increase in temperature is available as the temperature difference relative to ambient temperature, which can conveniently be measured directly using a thermopile between the suspended absorber and the bulk silicon. The characteristic feature of a thermocouple of measuring temperature difference rather than temperature makes the integrated system insensitive to variations in the temperature of the bulk of the chip. High sensitivity of an element in the thermopile-based IR detector requires minimum thermal conductance between the absorber and the heat sink. Micromachining technologies are generally employed for the removal of the thermal shunt of any bulk silicon underneath the TE detector for maximum sensitivity. These techniques and their effect on the sensitivity of IR detectors have been extensively studied [3, 4].

The lateral aspect ratio of a TE element is very large, which is due to the format of the image projected by the grating. This is a typical characteristic of the IR microspectrometer design and implies a large cross-sectional area between adjacent elements within the array and results in a relatively large heat exchange between elements in this lateral direction by thermal diffusion even in the case of the bulk silicon removed, which is referred to as thermal cross-talk. Therefore, heat exchange by conduction through the membrane support should be eliminated, which is achieved by cutting trenches in between TE elements. The shape of the resulting TE element is a bridge (absorption at middle) or a cantilever (absorption at tip) structure. A maximum optical revolving power implies a minimum element pitch. Hence, the spacing between two TE elements should be minimized for optical performance. However, the heat flux from one element to a neighbouring element by conduction through the surrounding gas increases with the decreasing gap. Therefore, a suitable design combines high spectral selectivity of the IR microspectrometer with

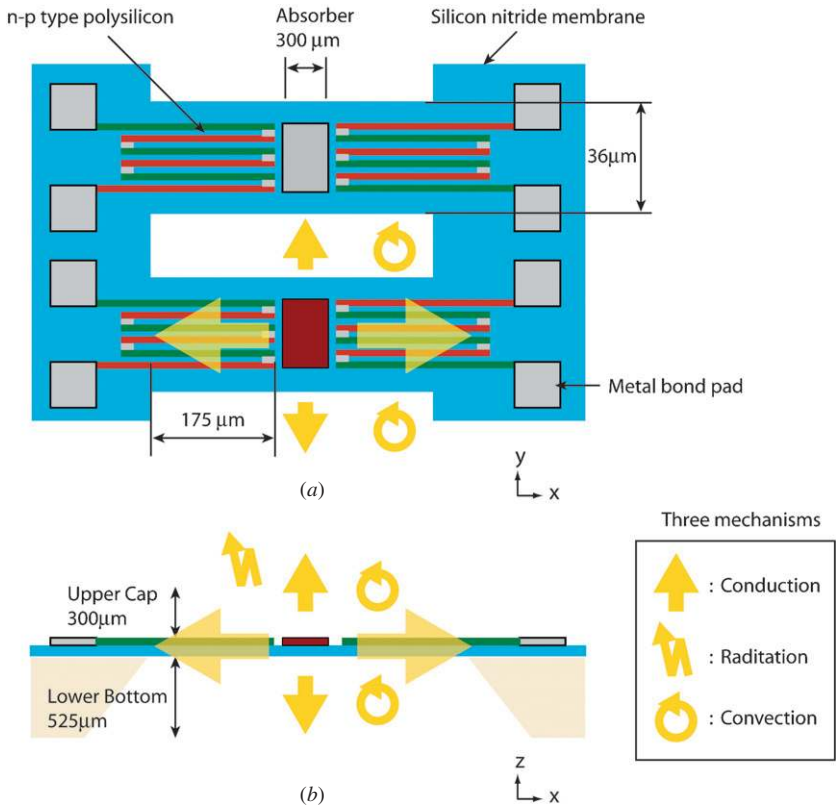

Figure 1. Heat transfer mechanisms in the thermopile bridge-shaped detector. (*a*) Two bridges are illustrated and the below bridge has the absorbed heat flux to transfer. (*b*) The cross-sectional view.

low thermal cross-talk between neighbouring TE elements. Although the challenges are similar to those introduced by the detrimental effect of a thermal shunt on sensitivity, this thermal cross-talk issue has not been addressed systematically and is the topic of this paper.

Figure 1 illustrates the configuration of the detector. The silicon nitride bridge structure acts as the support structure for the thermocouple, which is formed by the n–p-type polysilicon. The thermocouples convert the thermal energy from the projection light of grating via an absorber (middle of the bridge) into the voltage with the Seebeck effect. Conduction, convection and radiation are the three mechanisms of loss. The thermal transfer due to these three mechanisms acting on the TE element is also shown schematically in figure 1. All these loss mechanisms should be considered when analysing the sensitivity of a single element. Due to the aspect ratio of an element (small gap as compared to the sidewall area) only heat exchange between adjacent elements by conduction and convection is considered. The TE array is within an IC-compatible package. Therefore, the volume around an element is small, and the effect of gas pressure on the performance of the detector has to be considered. As is shown in this analysis, the gas conductivity determines the residual thermal cross-talk and, consequently, the lower limit of what can actually be achieved by the optimized design of the support structure and the structural separation of the elements.

The influence of heat exchange losses on the static detector response has been analysed using numerical methods. Thermal quadrupole models have been used for the simulation of the effect on the dynamic behaviour. The approach and results are presented in section 2. The fabrication for the process of the array with TE elements has been described before [2], however, is summarized in section 3 and employed for the fabrication of an array of 20 TE elements, each on a bridge structure of 650 × 36 μm^2. These devices have been used for validating the simulations and the experimental results are presented in section 4. These include sensitivity and cross-talk measurements at a range of air pressure levels that cover the heat exchange at both the molecular interaction regime and the viscous flow regime. Conclusions on the results and the effectiveness of the structural separation of TE detector are drawn in section 5.

2. Theory and the model

2.1. Thermal conductivity of air

For dimensions typical for packaged MEMS-based detectors the expression for thermal conductivity of air between two plates within an enclosed cavity as a function of pressure and temperature can be approximated as [5]

$$\kappa_{\text{air}} = \kappa_o \times \frac{1}{1 + \frac{7.6\times10^{-5}}{p\times\frac{D}{T_{\text{avg}}}}} \ (\text{W m}^{-1}\,\text{K}^{-1}), \tag{1}$$

where κ_{o}, p, D and T_{avg} denote the thermal conductivity of air at room pressure and temperature, the pressure, the distance between the plates and the average temperature of the plates,

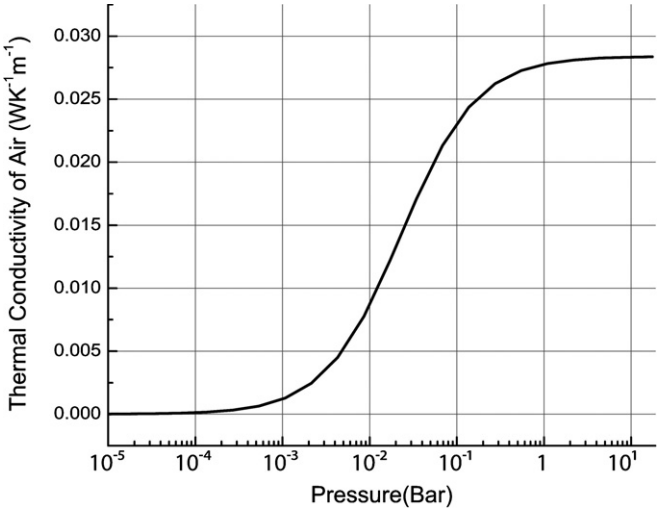

Figure 2. Air thermal conductivity as a function of pressure.

respectively. When assuming a plate spacing of 10 μm, an average temperature of 300 K and $\kappa_o = 0.0284$ W m^{-1} K^{-1}, a pressure-dependent thermal conductivity of air results as shown in figure 2.

2.2. *Theoretical considerations of the thermopile detector*

Operation of the infrared thermopile detector is based on the Seebeck effect. Radiation incident on the detectors heats up the absorption region and results in temperature gradient, which yields a Seebeck voltage. Analytical solutions for the heat conduction, which include convection and radiation losses, have been developed by assuming the direction of heat transfer in only one direction [4, 5]. There are three paths for the heat flow generated from radiant energy in the middle of the bridge-shaped thermo-electric detector. The first path is the heat conduction through the solid materials that comprise the suspension. The equivalent thickness and equivalent thermal conductivity of a multi-layers bridge can be expressed as

$$d_{\text{eq}} = \sum_{i=1}^{n} d_i(m), \tag{2}$$

$$\kappa_{\text{eq}} = \frac{1}{d_{\text{eq}}} \sum_{i=1}^{n} d_i \kappa_i (\text{W m}^{-1}\,\text{K}^{-1}), \tag{3}$$

where the d_i and κ_i denote the thickness of thin film and the thermal conductivity of material, respectively.

The second path is heat loss due to convection of heat from the detector surface to ambient, which can be neglected when considering the sensor package volume [6].

The final loss mechanism is due to the radiation effect and can be expressed as

$$4\sigma_B A(\varepsilon_u + \varepsilon_l) T_{\text{amb}}^3, \tag{4}$$

where σ_B is the Stefan–Boltzmann constant, A is the emission area (equal to the absorption area of an element), ε_u and ε_l are the emissivities of the upper and lower layers of emission area, respectively. This effect can in the first-order approximation be disregarded when considering the small value of the temperature increase, but is included in more accurate calculations.

Table 1. Thermal properties of material used for the simulation.

	Thermal conductivity (W m^{-1} K^{-1})	Specific heat (J kg^{-1} K^{-1})	Density (kg m^{-3})
Silicon nitride	1.55	170	2440
Polysilicon	25	700	2329
Silicon	130	700	2329

The dynamic response is governed by the Fourier equations, which is based on the heat transfer theory and is expressed as [7]

$$\rho C_p \frac{\partial T}{\partial t} + \nabla \cdot (-\kappa_{\text{eq}} \nabla T) = Q - \rho C_p \nabla T, \tag{5}$$

where ρ is the density of material, C_p is the specific heat capacity, and Q is the heat flux. This equation can be used for finding a simplified analytical expression of the sensitivity of a single element in a cavity. However, the device structure of a detector array with cross-talk is more complex. The detector array is designed and fabricated to have a fixed value of the gap width between elements. This is a two-dimensional problem with heat flux between several objects. Therefore, numerical methods are required. The commercially available finite element method (FEM) software, COMSOL [8], has been used to solve the heat transfer equation.

2.3. *Static response*

Several layers are stacked during the fabrication of the meander-shaped thermopile deposited on top of supporting membrane. Therefore, the equivalent parameters are calculated using equations (2), (3). Symmetry allows the simplification of the problem into three quarter-sized TE elements, which significantly reduces computational time. The 10 μm wide spacing between elements is modelled as air. The convection and radiation loss factors described in the previous section are included in the boundary conditions of the bridge surface. One element is given the constant heat flux in the middle position (the absorption area) of the bridge to create the temperature difference between the absorber to the bulk silicon where the temperature is constant. The temperature difference of the thermopile sensing area of the heated element is taken as the reference, while the temperature difference of two successive neighbouring elements indicates the cross-talk. The simulation result of cross-talk as a function of pressure, while assuming a constant ambient temperature at 300 K, is shown in figure 3. The thermal parameters used for simulation are listed in table 1. The cross-talk of the main pixel to the first side pixel is significant and is 5.16% at 1 bar (room pressure). The cross-talk towards only one side is calculated and the result should be multiplied by two for both sides. The figure demonstrates that the effect is significantly reduced when lowering the air pressure in the chamber in the device package. This is in agreement with the reduced effect of air conduction on the sensitivity of a single element. Cross-talk becomes negligible at air pressures below 10^{-5} bar. The cross-talk towards the next pixel (second in line) is about 0.13% at atmospheric pressure, which is due to the larger distance to

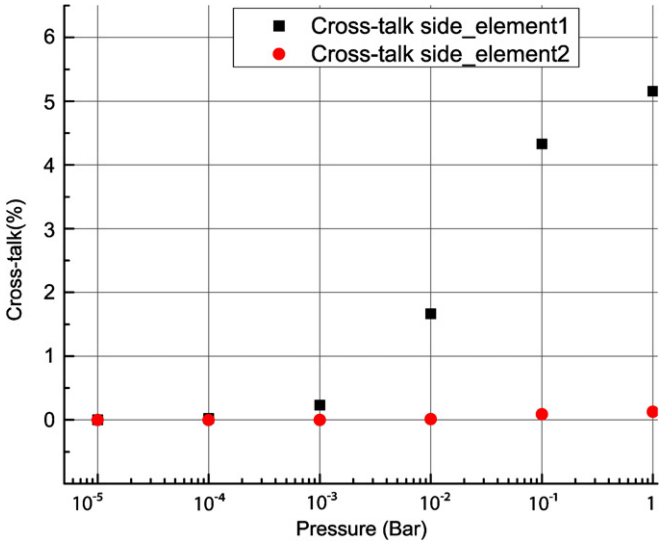

Figure 3. FEM simulation of cross-talk on three TE elements.

the heated element. Therefore, this effect can be disregarded and only the two directly neighbouring elements need to be considered.

2.4. Dynamic response

The dynamic response of the thermal detector array is related to the thermal time constant of the detector and, thus, depends on the equivalent heat capacitance of the bridge with materials on top and should be calculated using

$$C_{\text{eq}} = \sum_{i=1}^{n} V_i \rho_i c_i \,(\text{J K}^{-1}), \tag{6}$$

where V_i, ρ_i and c_i denotes the volume of the material, density of the material and the specific heat capacity of the material, respectively.

Although the transient simulation on the heat transfer can be achieved by the FEM, the long computational time makes it impractical to use the FEM for design optimization and the detector element has been expressed in terms of quadrupoles instead. The representation in quadrupoles basically allows a reduction of the dimension of the problem, and the one-dimensional heat transfer equation, as is shown in equation (5) in the Laplace domain, can subsequently be used [9, 10]. Equations (2)–(4), (6) are used to calculate the equivalent parameters of the bridge and are applied to the matrix coefficients (*A, B, C* and *D*) in such a way that the linear, passive and isotropic layer result is obtained:

$$\begin{pmatrix} \theta_{\text{in}} \\ \phi_{\text{in}} \end{pmatrix} = \begin{pmatrix} A & B \\ C & D \end{pmatrix} \begin{pmatrix} \theta_{\text{out}} \\ \phi_{\text{out}} \end{pmatrix}$$
$$= \begin{pmatrix} \cosh\left(\sqrt{\frac{j\omega}{q}}L\right) & \frac{1}{\kappa\sqrt{\frac{j\omega}{q}}A}\sinh\left(\sqrt{\frac{j\omega}{q}}L\right) \\ \kappa\sqrt{\frac{j\omega}{q}}A\sinh\left(\sqrt{\frac{j\omega}{q}}L\right) & \cosh\left(\sqrt{\frac{j\omega}{q}}L\right) \end{pmatrix}$$
$$\times \begin{pmatrix} \theta_{\text{out}} \\ \phi_{\text{out}} \end{pmatrix}, \tag{7}$$

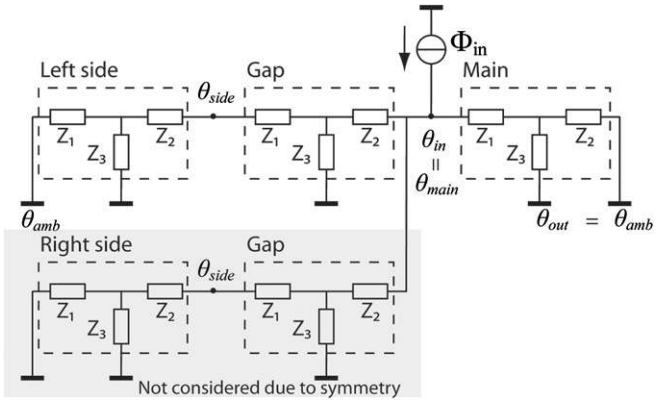

Figure 4. Thermal quadrupole models of neighbouring elements with one gap spacing.

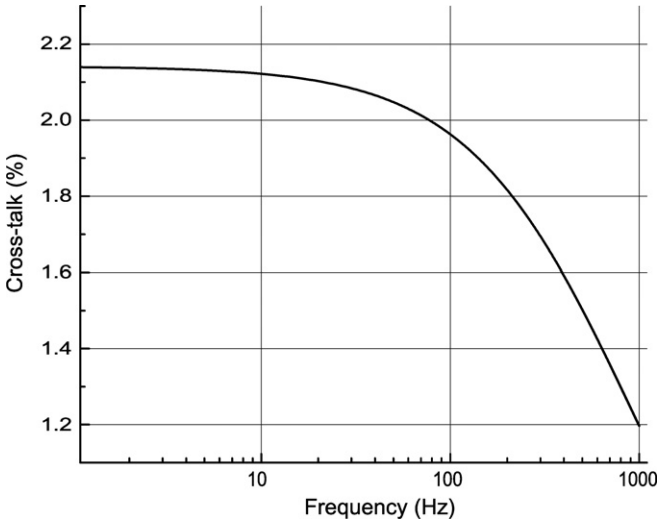

Figure 5. Thermal modulus plot of the cross-talk at 9.3 mbar pressure.

where θ_{in} and θ_{out} are the input and output Laplace temperatures, respectively, ϕ_{in} and ϕ_{out} are the input and the output Laplace heat flux, respectively, $j\omega$ is the Laplace variable, L is the length of the bridge, q is the thermal diffusivity and expressed by $\kappa/\rho c$, A is the cross-sectional area of the bridge along the length coordination.

Since the matrix is linear and reversible, it can be considered as the mathematical representation of the transfer function of the network composed of three thermal impedances in a 'T' shaped circuit with $Z_1 = Z_2 = (A-1)/C$, $Z_3 = 1/C$. Each bridge and air gap can be represented as a single quadrupole model as shown in figure 4. Due to the symmetry of the configuration, only the part left or right from the main element needs to be considered.

The modulus of the thermal cross-talk is expressed in terms of the temperature increase of the neighbouring element relative to that of the heated element itself. The dynamic response of cross-talk to the side element (figure 4) at 9.3 mbar pressure is shown in figure 5. The modulus of the thermal response of the heated (main) pixel as a function of packaging pressure is presented in the experiment section and compared to the measurement result. As having the similar trend in the FEM simulation, the simulation result shows that the dc

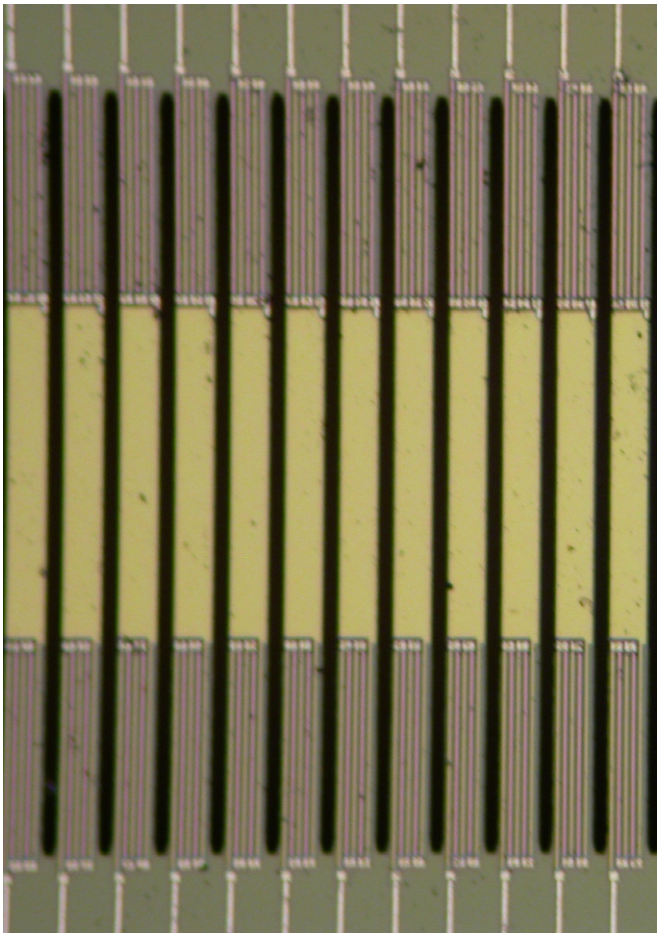

Figure 6. View of bridges in the middle section of the array.

sensitivity is improved by decreasing the air pressure and is in agreement with the literature.

3. Device fabrication

The bridge was designed to have a 300 × 36 μm^2 absorption area with a 350 × 36 μm^2 sensing area. Five thermocouples with 4 μm wide thermal legs of polysilicon are placed to cover the entire available sensing area of the bridge. Each of thermal legs has 2 μm spacing for separation.

Fabrication was based on a CMOS process followed by a backside bulk-micromachining step. Wafer processing started with a 800 nm of low stress SiN film formation using LPCVD as the function of the supporting membrane. Implanted polysilicon layers of 300 nm thickness have been used as the thermo-electric materials. RIE has been used for the formation of thermocouples. A 100 nm low-stress silicon nitride layer was deposited on top of the membrane as the passivation layer in between 600 nm aluminium and polysilicon. The next step is to cut the 10 μm wide trench between elements, which was etched to 21 μm depth. A silicon layer of variable thickness up to 21 μm was left underneath the bridges and used for experimenting with the compromise between improved mechanical strength at larger thickness versus loss of sensitivity due to increased thermal

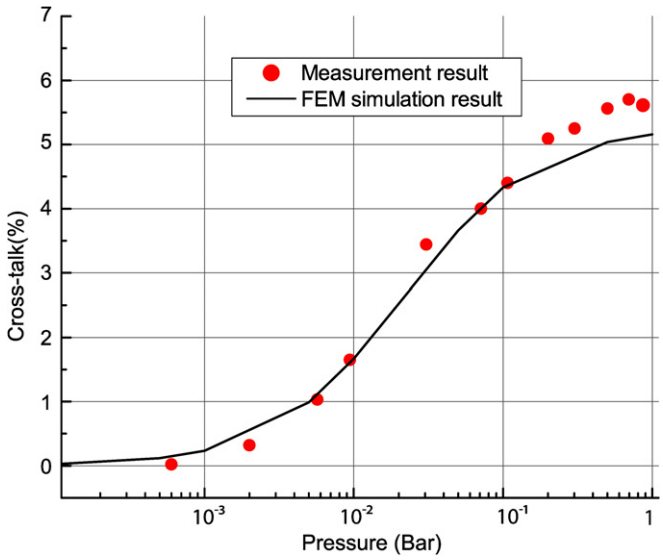

Figure 7. Cross-talk (on single side) measurement of elements under different pressures.

conductivity through the bridge suspension. In the final step, the wafers were processed with KOH wet etching to make the membranes for limiting cross-talk. The final detector array has a sandwiched bridge structure which includes 100 nm passivation SiN, 300 nm thick polySi–polySi thermopiles, a 800 nm thick nitride layer and up to 20 μm thick bulk silicon. Figure 6 shows the completed thermopile array with a dimension of 650 × 36 μm^2 and 10 μm wide trenches between bridges.

4. Experimental results

Thermal cross-talk between two TE elements in the array with 10 μm wide trenches has been measured in a vacuum chamber using a 14 μm diameter He–Ne laser spot (FWHM), which is chopped at a frequency of 2 Hz. The spot is projected on one element and the resulting Seebeck voltage is measured using a HP 34420 A nano-voltmeter. Simultaneously, the Seebeck voltage of the neighbouring element is recorded. The experimental result of cross-talk as a function of air pressure is presented in figure 7. The results indicate that cross-talk is determined by both thermal heat leakage through the gap to the neighbourhood element and also on the optical leakage from the laser spot contributes the cross-talk.

The optical cross-talk is inherent to the measurement technique. First, the scattering light due to the uncompleted absorption of the main pixel is reflected from the bottom plate of packaging to the side pixels. Second, the glass cap of the vacuum chamber directly on top of the chip results in some scattering in the laser light. The optical light leakage is determined in a separate measurement at very low air pressure, where the cross-talk due to heat transfer is assumed negligible. The corrected result is in good agreement with the FEM simulation result. The deviation at higher pressures is due to convection.

An extension of this measurement technique has been used for measuring the dynamic thermal response of both the

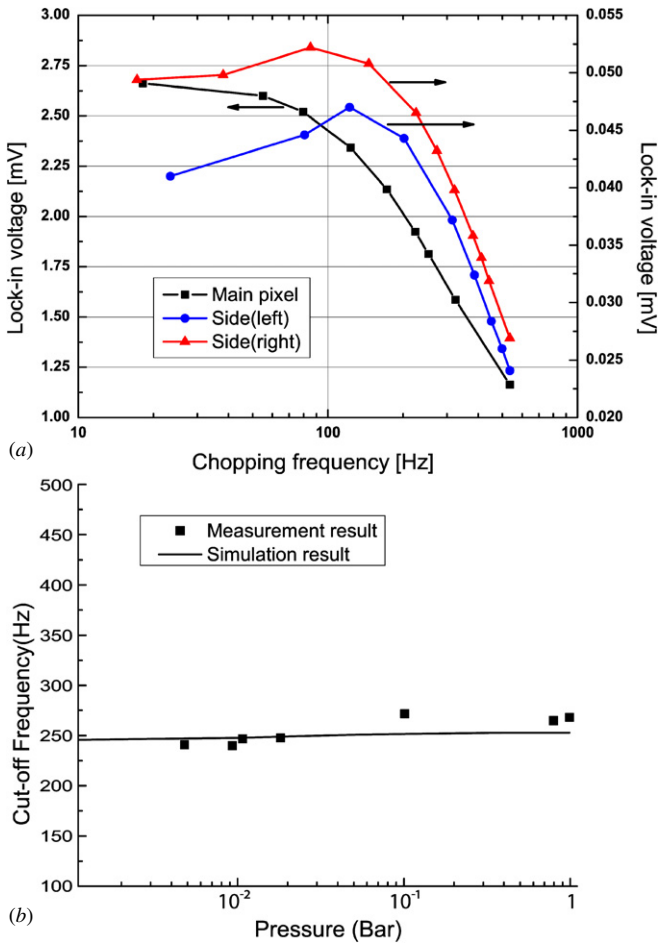

Figure 8. (*a*) Thermal modulus plot of three elements at 1 mbar pressure. (*b*) Cut-off frequency of heated element under different pressures.

single element and the thermal cross-talk between elements. The laser spot is frequency modulated for this purpose. The measurement setup includes the He–Ne laser, the optical chopper, the vacuum chamber, lock-in amplifier SR830 for measuring the thermal modulus plot and the digital oscilloscope for recording the thermal time constant to validate the ac response. The thermal modulus plot of three elements with the heated (illuminated) pixel in the middle at 1 mbar is shown in figure 8(*a*). The measured thermal cross-talk (corrected for optical leakage) is 0.4% (single side), which is in agreement with the simulation. The cut-off frequency of the main pixel and side pixel in the measurement of atmosphere pressure is at 240 Hz and 183 Hz, respectively. The cut-off frequency of the side pixel is lower than that of the heated pixel due to the higher thermal resistance of the air gap. The cut-off frequencies are not significantly affected by air pressure, as is demonstrated by figure 8(*b*).

5. Conclusions and future work

The theoretical analysis, modelling and experimental validation of the thermal cross-talk in a CMOS compatible thermopile array for use in a miniaturized infrared microspectrometer are presented. A process flow has been used that allows the fabrication of such an array with a gap spacing of 10 μm between elements, which limits thermal cross-talk from one element to the two neighbouring elements to 10.3% when operated at atmospheric pressure. This is not acceptable in practical device operation. A wider trench between elements helps to decrease cross-talk, but is not an acceptable solution when also considering optical resolving power [2]. A more effective solution is to operate the array at reduced air pressure, which also contributes to the sensitivity of each thermopile element.

A FEM analysis has been applied to estimate the performance of the dc sensitivity and cross-talk and the results are experimentally validated. The residual thermal cross-talk is measured at 1 mbar to be 0.8%, which is in good agreement with the modelling and acceptable in the IR microspectrometer. The FEM method is not suitable for the dynamic analysis and the thermal quadrupole model has been used instead. The bandwidth at the given dimensions was at 240 Hz for the radiated main element due to its suspension and at 183 Hz for the side element due to cross-talk. This result is in good agreement with simulations, which also indicate a pressure-independent cut-off frequency. Convection losses have been observed at pressure levels beyond 100 mbar.

The measurement results do validate the model, while these reveal a deviation at the higher end of the pressure range, which is due to convection. In future work, the convection effect through gap should be included and analysed to have a more accuracy model. Devices of slightly different dimensions will be fabricated to study the effect of process variations on the performance. The packaging becomes simpler in case the air pressure can be kept at a higher level. Therefore, a design optimization for operation at e.g. 10 mbar is considered. Furthermore, the hybrid integration of optimized grating and detector part in a package and the on-chip integration of TE elements and detector array readout circuitry to yield a fully-integrated IR microspectrometer are topics of further research.

Acknowledgments

This work has been supported in part by the Dutch technology foundation STW under grant DET.6667. Devices have been fabricated at the DIMES (Delft Institute of Microsystems and Nanoelectronics). The authors are indebted to W van der Vlist for his assistance in device fabrication and to P M Sarro for helpful discussions on the processing.

References

[1] Wolffenbuttel R F 2005 MEMS-based optical mini- and microspectrometers for the visible and infrared spectral range *J. Micromech. Microeng.* **15** S145–52
[2] Wu H, Grabarnik S, Emadi A, de Graaf G and Wolffenbuttel R F 2008 A thermopile detector array with scaled TE elements for use in an integrated IR micro-spectrometer *J. Micromech. Microeng.* **18** 064017
[3] *Fluid Flow Databook* 1982 General Electric Section 410.2
[4] Volklein F and Baltes H 1993 Optimization tool for the performance parameters of thermoelectric microsensors *Sensors Actuators* A **36** 65–71

[5] Escriba C, Campo E, Esteve D and Fourniols J Y 2005 Complete analytical modeling and analysis of micromachined thermoelectric uncooled IR sensors *Sensors Actuators* A **120** 267–76

[6] Pitts D and Sissom L 1998 *Schaum's Outline of Theory and Problems of Heat Transfer* (New York: McGraw-Hill)

[7] Incropera F P and De Witt D P 1990 *Fundamentals of Heat and Mass Transfer* (Toronto: Wiley)

[8] COMSOL Multiphysics 3.4 2008 COMSOL Inc. http://www.comsol.com/

[9] Maillet D, André S, Batsale J C, Degiovanni A and Moyne C 2000 *Thermal Quadrupoles: Solving the Heat Equation through Integral Transforms* (New York: Wiley)

[10] André S, Rémy B, Maillet D, Degiovanni A and Serra J-J 2004 Modulated photothermal radiometry applied to semitransparent samples: models and experiments *J. Appl. Phys.* **96** 2566